JPE 19-2-20

https://doi.org/10.6113/JPE.2019.19.2.549
ISSN(Print): 1598-2092 / ISSN(Online): 2093-4718

Adaptive Sliding Mode Control with Enhanced Optimal Reaching Law for Boost Converter Based Hybrid Power Sources in Electric Vehicles

Bin Wang*, Chaohui Wang†**, Qiao Hu*, Guangliang Ma**, and Jiahui Zhou**

†,*Shaanxi Key Laboratory of Intelligent Robots, Xi'an Jiaotong University, Xi'an, China
**State Key Laboratory for Manufacturing Systems Engineering, Xi'an Jiaotong University, Xi'an, China

Abstract

This paper proposes an adaptive sliding mode control (ASMC) strategy with an enhanced optimal reaching law (EORL) for the robust current tracking control of the boost converter based hybrid power source (HPS) in an electric vehicle (EV). A conventional ASMC strategy based on state observers and the hysteresis control method is used to realize the current tracking control for the boost converter based HPS. Then a novel enhanced exponential reaching law is proposed to improve the ASMC. Moreover, an enhanced exponential reaching law is optimized by particle swarm optimization. Finally, the adaptive control factor is redesigned based on the EORL. Simulations and experiments are established to validate the ASMC strategy with the EORL. Results show that the ASMC strategy with the EORL has an excellent current tracking control effect for the boost converter based HPS. When compared with the conventional ASMC strategy, the convergence time of the ASMC strategy with the EORL can be effectively improved. In EV applications, the ASMC strategy with the EORL can achieve robust current tracking control of the boost converter based HPS. It can guarantee the active and stable power distribution for boost converter based HPS.

Key words: Adaptive sliding mode control, Boost converter, Electric vehicle, Hybrid power source, Particle warm optimization

I. INTRODUCTION

Hybrid power sources (HPSs), which consist of batteries and supercapacitors (SCs), have significant performance advantages in terms of high-power density and high energy density [1], [2]. HPSs have been extensively used in electric vehicles (EVs) [3], [4], electric urban buses [5], hybrid EVs [6], etc. Generally, HPSs use DC-DC converters such as buck, boost and buck-boost to connect batteries and SCs [2], [7]-[9]. From all of these HPSs, boost converter based HPSs can provide a high-voltage output to reduce the system energy losses of the electric drive systems in EVs or hybrid EVs [2], [10], [11]. At the high-voltage output side of boost converter based HPSs, SCs can directly absorb extra energy or provide peak power to motor inverters. As a result, batteries can be isolated from the high frequency charge-discharge at the low-voltage side so they can be easily managed [3], [4]. For the boost converter based HPSs in EVs, the output current of the batteries can be regulated with the boost converter, which achieves an active and stable power distribution between batteries and SCs [12]. Hence, robust current tracking control of the boost converter is of critical importance for boost converter based HPSs [13], [14]. To ensure robust current control and to achieve active power distribution between the batteries and the SCs, the control strategy should deal with the un-modeled dynamics and unknown disturbances of boost converter based HPSs [3].

It is very challenging to design control strategies for the boost converter based HPSs in EVs since un-modeled dynamics and disturbances of the boost converter cannot be accurately estimated [3], [15]. In addition, the SC pack is paralleled with the load. It can be considered as a variable load at the output side of the boost converter [3]. If a controller of a boost converter is designed based on the conventional

Manuscript received Jul. 16, 2018; accepted Dec. 14, 2018
Recommended for publication by Associate Editor Hongfei Wu.
†Corresponding Author: chhw@xjtu.edu.cn
Tel: +86-29-82663013, Xi'an Jiaotong University
*Shaanxi Key Lab. Intelligent Robots, Xi'an Jiaotong Univ., China
**State Key Lab. Manufacturing Syst. Eng., Xi'an Jiaotong Univ., China

proportional-integral (PI) control strategy, the overall system stability of the boost converter based HPS might not be guaranteed [4], [16]. For instance, a PI controller can achieve high-performance current control for a boost converter based HPS under some constant operating conditions [4]. However, if the reference current demand of the boost converter based HPS is changed, system parameter variations occur. In this condition, the PI controller cannot adaptively adjust its control factors in accordance with the parameter variations. Therefore, fuzzy logic and neural network (NN) strategies were developed to improve the PI control strategy [17], [18]. However, the fuzzy logic strategy was designed on the basis of a limited number of rules [19]. The effectiveness of this strategy should be enhanced by using other optimization methods. For the NN strategy used in boost converter based HPSs, the boundary layer design is a big problem [18]. The boundary layer should be designed based on unknown disturbances and un-modeled dynamics. As a result, the NN strategy can be very complex.

In EV applications, it is expected that the control strategies can be simply and effectively implemented in boost converter based HPSs. To simplify the current tracking control strategy of the boost converter based HPS, sliding mode control (SMC) strategies can be introduced to improve the PI control strategy [4]. In previous studies, various SMC strategies based on the PI control strategy have been successfully developed for the current tracking control of DC-DC converters [3], [4], [20]. These strategies can also be introduced into the current tracking control of boost converter based HPSs, since SMC controllers can improve the system robustness with an invariance property to deal with system uncertainties and un-modeled dynamics [21]-[23]. For instance, a SMC with a multi-resonant sliding surface has been successfully used to deal with system parameter variations [22]. On the other hand, the adaptive SMC (ASMC) strategy was designed based on state observers, which can effectively estimate load variations and unknown external input voltage [23]. This strategy can achieve a robust current control for boost converters. However, the sliding surface was designed without an integral item. In [3], the sliding surface of the SMC strategy was redesigned with an integral item of the current error to achieve a better current tracking control effect for the boost converter based HPS. The convergence time of the current adjustment can be improved with the redesigned sliding surface. For the SMC based on the PI control strategy, the control parameters can be more easily obtained according to the Lyapunov function [9], [24], [25]. The system stability can be guaranteed when the system state reaches the sliding surface [17], [26].

For SMC controllers, the chattering problem caused by the uncontrollable infinite switching frequency of sign functions cannot be ignored [3], [20]. If this problem cannot be addressed in boost converter based HPS applications, regular current management of the battery pack cannot be assured. As a result, battery degradation cannot be avoided [27]. What is worse, the infinite switching frequency might damage the MOSFET switches of the boost converter [4]. In previous studies, SMCs with the H2/H∞ control method can achieve a constant switching frequency [28]. In addition, hysteresis control (HC) methods can alleviate the switching frequency [9], [29]. However, the convergence time of SMC systems based on HC cannot be effectively improved. Although the total SMC method can be used to improve the convergence time, the lumped uncertainties of the SMC system should be effectively estimated [30]. In [20], the convergence problem was successfully resolved. Fractional power was adopted in the reaching law of the SMC strategy to deal with the voltage feedback error, which improves the system convergence time. The fractional power included in the sliding surface has an effect that is similar to that of exponential reaching laws, which can achieve a fast response speed when the system state is far away from the sliding surface [31]. However, this can also reduce the response speed when the system state is close to the sliding surface. Therefore, the fractional power of the reaching law should be optimized according to the different states of the sliding surface.

Particle swarm optimization (PSO) algorithms can be a good choice for optimizing the reaching law [32], [33]. When compared with other optimization algorithms, PSO algorithms use multiple particle swarms rather than one particle to achieve a multi-direction search for the optimal solution [34], [35]. Therefore, the search results quickly converge to the optimum solution. In addition, PSO algorithms are also very suitable for the combination optimizations in practical applications [31], [35].

In this paper, an ASMC strategy with an enhanced optimal reaching law (EORL) is proposed for the robust current tracking control of the boost converter based HPSs in EVs. The main contribution of the proposed ASMC strategy is that the enhanced exponential reaching law is optimized by a PSO algorithm. In addition, both the start-up and load variation conditions of the boost converter based HPS are considered for designing the PSO algorithm. Therefore, the system stability of the boost converter based HPS can be guaranteed under start-up and load variation conditions. The remainder of this paper is organized as follows. In Section II, an average state-space model of a boost converter based HPS is established. Then, an ASMC strategy based on state observers and the HC method is introduced in Section III. Section IV presents the EORL design of the ASMC strategy. Simulation and experimental results are discussed in Section V. Finally, conclusions are given in Section VI.

II. Model of a Boost Converter Based HPS

Fig. 1 shows the boost converter based HPS and its control scheme. It can be seen that the boost converter is the only actuator for energy management of the boost converter based HPS. The power-split supervisory controller gathers information

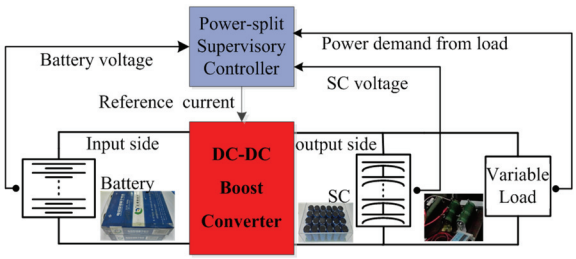

Fig. 1. Boost converter based HPS and its control scheme.

of the battery voltage, the SC voltage and the load to calculate the reference current of the boost converter.

By considering the input voltage and load variations, the average state-space model of the boost converter based HPS can be expressed as:

$$\dot{x}_1 = -\frac{(1-d)}{L}x_2 + \frac{1}{L}(V_{\text{in}} + \Delta V_{\text{in}}) \tag{1}$$

$$\dot{x}_2 = \frac{(1-d)}{C}x_1 - \frac{1}{(R+\Delta R)C}x_2 \tag{2}$$

where x_1 is the average inductor current, $d \in (0,1)$ is the control factor, x_2 is the average output voltage, and L and C represent the inductance and capacitance, respectively. ΔV_{in} and ΔR represent variations of the input voltage V_{in} and the load R, respectively.

By using V'_{in} and G' to replace the terms $(V_{\text{in}} + \Delta V_{\text{in}})$ and $1/(R+\Delta R)$, (1) and (2) can be simplified as:

$$\dot{x}_1 = -\frac{(1-d)}{L}x_2 + \frac{V'_{in}}{L} \tag{3}$$

$$\dot{x}_2 = \frac{(1-d)}{C}x_1 - \frac{G'}{C}x_2 \tag{4}$$

It should be noticed that (3) and (4) are similar to the average state-space model of the boost converter. The differences are the un-modeled dynamics and disturbances of the boost converter based HPS. Thus, these differences should be considered when designing the ASMC strategy.

III. ASMC Based on State Observers and HC

Define the following sliding surface:

$$s = (x_1 - \hat{x}_1) + \lambda \int_0^t (x_1 - \hat{x}_1)\, dt \tag{5}$$

where k_1 and λ are positive constants, and $\hat{x}_1 = V_{\text{ref}}^2 \hat{G}' / \hat{V}'_{in}$ represents the estimate value of x_1, $x_1 - \hat{x}_1 = \tilde{x}_1$.

The conventional reaching law is designed as $u_{SMC} = \dot{s} = -ks(t) - \rho \text{sgn}(s(t))$ so that $s\dot{s} < 0$ can be guaranteed. With this design, it is possible to obtain $-ks(t) - \rho \text{sgn}(s(t)) = -\frac{(1-d)}{L}x_2 + \frac{1}{L}V'_{in} - \dot{\hat{x}}_1 + \lambda \tilde{x}_1$. Therefore, the average control factor can be calculated as follows.

$$d = 1 - \frac{-Lu_{SMC} + L(V_{\text{ref}}^2 \hat{G}' \dot{\hat{V}}'_{in} / \hat{V}'^2_{in} - V_{\text{ref}}^2 \dot{\hat{G}}' / \hat{V}'_{in}) + \lambda L \tilde{x}_1 + V'_{in}}{x_2} \tag{6}$$

To calculate $\dot{\hat{V}}'$ and $\dot{\hat{G}}'$, the state observers are defined as follows [3].

$$\dot{\hat{x}}_1 = -\frac{(1-d)}{L}\hat{x}_2 + \frac{\hat{V}'_{in}}{L} + \alpha_1(x_1 - \hat{x}_1) \tag{7}$$

$$\dot{\hat{x}}_2 = \frac{(1-d)}{C}\hat{x}_1 - \frac{\hat{G}'}{C}\hat{x}_2 + \alpha_2(x_2 - \hat{x}_2) \tag{8}$$

Based on the state observers and the average state-space model of the boost converter based HPS, the adaptive laws can be derived as follows [3].

$$\dot{\hat{G}}' = -\beta_1 x_2 \tilde{x}_2, \quad \dot{\hat{V}}'_{in} = \beta_2 \tilde{x}_1 \tag{9}$$

To show the stabilization of the ASMC system, the Lyapunov function is selected as:

$$V = \frac{1}{2}L\tilde{x}_1^2 + \frac{1}{2}C\tilde{x}_2^2 + \frac{1}{2\beta_1}\tilde{G}'^2 + \frac{1}{2\beta_2}\tilde{V}'^2_{in} \tag{10}$$

The derivative of V can be expressed as follows [3].

$$\dot{V} = -\alpha_1 L\tilde{x}_1^2 - \alpha_2 C\tilde{x}_2^2 - \hat{G}'\tilde{x}_2^2 - \tilde{G}'[x_2\tilde{x}_2 + \frac{\dot{\hat{G}}'}{\beta_1}] + \tilde{V}'_{in}[\tilde{x}_1 - \frac{\dot{\hat{V}}'_{in}}{\beta_2}] \tag{11}$$

According to (9) and (11), there is no doubt that $\dot{V} < 0$. Therefore, the system stability can be guaranteed.

By combining (6) and (9), the adaptive control factor can be calculated as:

$$d = 1 - \frac{\lambda L\tilde{x}_1 + V'_{in} - Lu_{SMC} + LV_{\text{ref}}^2(\hat{G}'\beta_2\tilde{x}_1 / \hat{V}'^2_{in} + \beta_1 x_2 \tilde{x}_2 / \hat{V}'_{in})}{x_2} \tag{12}$$

Notice that the sign function $\rho \text{sgn}(s(t))$ in the item $u_{SMC} = -ks(t) - \rho \text{sgn}(s(t))$ may lead to a chattering deviation, which is a drawback of the system stability. To reduce system chattering, the HC method is used to manage the sign function $\text{sgn}(s(t))$, as shown in Fig. 2. With this design, the sign function can be eliminated if $|s(t)| \le 0.01$. This can effectively reduce the system chattering caused by $\rho \text{sgn}(s(t))$. Moreover, the control precision cannot be degraded since $|s(t)|$ is very small and has little adverse effect on the control system. If $|s(t)| \ge 0.1$, the sign function can be activated to improve the regulation speed of the ASMC controller.

In previous studies, both boundary control and HC methods were introduced to solve the chattering problem [4], [17], [36]. However, for the boundary control, the stability inside the boundary layer cannot be assured [17]. Based on the above analysis, the HC method is chosen to deal with the sign function so that the chattering phenomena caused by $\rho \text{sgn}(s(t))$ can be effectively suppressed.

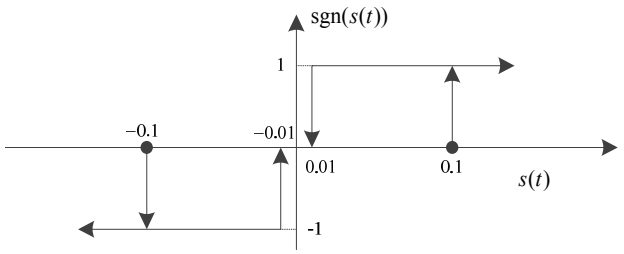

Fig. 2. HC design for the sign function.

IV. ASMC WITH THE OPTIMAL REACHING LAW

A. A. Redesign of the Reaching Law

The reaching law design is very important for the transient response of ASMC controllers. For the conventional ASMC strategy, the reaching law is $u_{SMC}=\dot{s}=-ks(t)-\rho\,\mathrm{sgn}(s(t))$. However, the conventional reaching law cannot reflect the control effect of fractional power. In [20], the fractional power is introduced into the reaching law to improve the convergence time. It can improve the response speed of the current control during load changes. The fractional power can also be introduced to design enhanced exponential reaching laws. In this paper, the proposed reaching law is:

$$u_{SMC}=\dot{s}=-k_1 s^{\alpha}-k_2|s|^{\beta}\,\mathrm{sgn}(s)-\varepsilon\,\mathrm{sgn}(s) \tag{13}$$

where k_1, $k_2>0$, $0<\beta<1$ is the fractional power, and α should be designed with a positive odd integer.

The proposed reaching law can be divided into two parts, i.e., $\dot{s}_1=-k_1 s^{\alpha}-\varepsilon\,\mathrm{sgn}(s)$ and $\dot{s}_2=-k_2|s|^{\beta}\,\mathrm{sgn}(s)$. Therefore, the redesigned reaching law can also satisfy $s\dot{s}<0$. The fractional power in the exponential reaching law $\dot{s}_2=-k_2|s|^{\beta}\,\mathrm{sgn}(s)$ can be used to improve the response speed when the system state is far from the sliding surface. On the other hand, it can also reduce the response speed when the system state is close to the sliding surface. However, the integer power in the exponential reaching law $\dot{s}_1=-k_1 s^{\alpha}-\varepsilon\,\mathrm{sgn}(s)$ can compensate the control effect. Based on the redesigned reaching law, the final adaptive control factor can be calculated as:

$$d=1-\frac{L(k_1 s^{\alpha}+k_2|s|^{\beta}\,\mathrm{sgn}(s)+\varepsilon\,\mathrm{sgn}(s)+\lambda\tilde{x}_1)}{x_2}-\frac{V'_{in}-LV_{\mathrm{ref}}^2(-\hat{G}'\beta_2\tilde{x}_1/\hat{V}'^2_{in}-\beta_1 x_2\tilde{x}_2/\hat{V}'_{in})}{x_2} \tag{14}$$

According to (14), a constant-frequency PWM signal can be used to control the MOSFET of the boost converter. That is to say, the sliding mode controller is used to calculate the final adaptive control factor to control the MOSFET of the boost converter. Therefore, the uncontrollable infinite switching frequency of the duty ratio caused by chattering can be avoided. Moreover, the HC function is used to deal with the sign function $\mathrm{sgn}(s(t))$, as shown in Fig. 2. When $|s(t)|\le 0.01$, the reaching law in (13) is changed to $u_{SMC}=-ks(t)$, which does not have the sign function. With this design, the chattering phenomena of the duty ratio caused by the sign function can be effectively suppressed.

For the sliding surface in (14), a non-linear sliding surface design with an exponential term might lead to a better control effect when compared with the conventional sliding surface. However, the non-linear sliding surface might lead to a singularity problem. Therefore, a conventional sliding surface with an integral term is designed. To have a similar control effect to that of a non-linear sliding surface, the reaching law in (13) is designed with exponential terms. Notice that the design of the exponential gains α and β is related to the convergence time. For example, the fractional power in the exponential reaching law $\dot{s}_2=-k_2|s|^{\beta}\,\mathrm{sgn}(s)$ can be used to improve the convergence time when the system state is far from the sliding surface, while it can also reduce the response speed when the system state is close to the sliding surface [31]. In addition, the exponential gains α and β can affect the current amplitude irregularly. Therefore, PSO is used to optimize the exponential gains and to improve the convergence time.

B. Optimization of the Reaching Law

The redesigned reaching law in (13) includes an integer power part and a fractional power part. Five parameters, i.e., three control gains (k_1, k_2 and ε) and two exponential gains (α and β) should be designed. In practical applications, k_1, k_2 and ε can affect the convergence time and the current amplitude of the boost converter based HPS. Although a large value design of the parameters k_1, k_2 and ε can improve the convergence time, a large current amplitude caused by the large value design of k_1 and k_2 as well as the chattering phenomena caused by the sign function $\varepsilon\,\mathrm{sgn}(s)$ might occur. Actually, k_1 and k_2 can be designed according to the PI algorithm. ε should be conservatively designed [4].

The key to the design is to define the exponential gains α and β. Simulation results of the boost converter based HPS controlled by the ASMC strategy with different designs of α and β are shown in Fig. 3. It can be seen that the exponential gains have an obvious effect on the system dynamic response.

In Fig. 3, a high current amplitude occurs when the two exponential gains are designed as $\alpha=7$ and $\beta=0.5$. As a comparison, the current amplitude can be significantly improved when the two exponential gains are designed as $\alpha=3$ and $\beta=0.37$. However, it can be known from Fig. 3 that the current amplitude cannot be regularly improved by

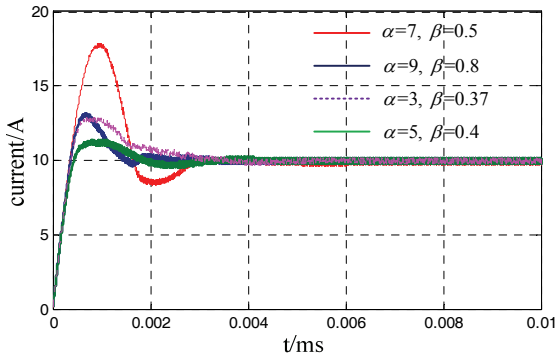

Fig. 3. Simulations based on different designs of α and β.

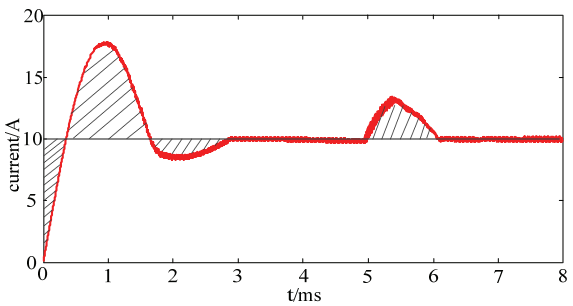

Fig. 4. Physical significance of the PSO goal function.

increasing or decreasing the two exponential gains. In fact, the two exponential gains can irregularly affect the current amplitude. Therefore, the two exponential gains should be optimized with a stochastic optimization algorithm.

The PSO algorithm is a good stochastic optimization algorithm [34], [35]. This algorithm uses multiple particle swarms to achieve a multi-direction search for the optimal solution. Therefore, the search results quickly converge to the optimum solution. It is known that the two exponential gains in the reaching law affect both the current amplitude and the convergence time. Therefore, the global optimization goal of the PSO algorithm in this paper is designed as:

$$f(\alpha^*,\beta^*)=min(\int_0^t |x_1-x_1^{target}|dt) \quad (15)$$

where α^* and β^* are the optimal values of α and β, and x_1^{target} is the target value of x_1. t is the convergence time of the proposed ASMC system.

The PSO goal function is designed based on the real-time error of x_1 and the convergence time. It should be noticed that both start-up and load variation conditions are considered for the PSO algorithm. According to [4] and [9], if the ASMC strategy can deal with un-modeled dynamics and unknown disturbances of the boost converter based HPS under start-up and load variation conditions, the output current accurately tracks the reference current even if the reference current is continuously changed. The physical significance is shown in Fig. 4. The final goal is to obtain the smallest shaded area.

For each particle i and dimension j of the proposed

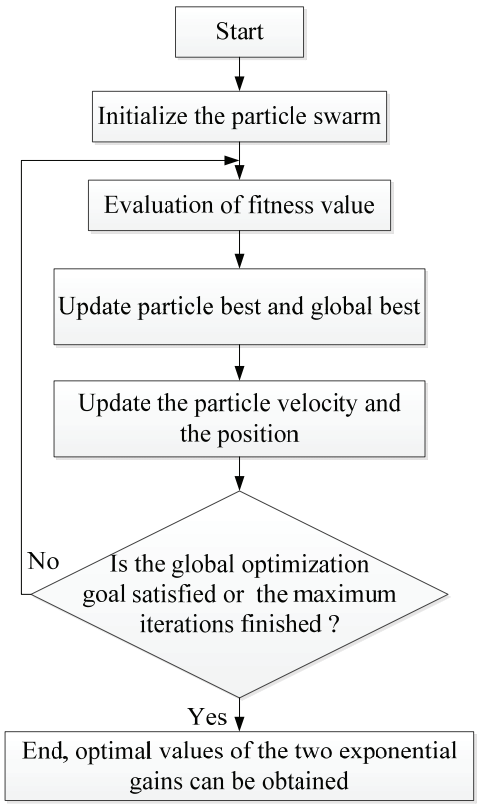

Fig. 5. Flow chart of a PSO algorithm.

PSO algorithm, the velocity and position of the particles can be updated as:

$$v_{ij}^{k+1}=\omega v_{ij}^k+c_1 rand(pbest_{ij}^k-x_{ij}^k)+c_2 rand(gbest_{ij}^k-x_{ij}^k) \quad (16)$$

$$x_{ij}^{k+1}=x_{ij}^k+\lambda v_{ij}^{k+1} \quad (17)$$

Step 1: The particle swarm of the PSO algorithm is initialized with a population of random particles and velocities. α is designed in the region [1], [11], while β is designed in the region [0.01, 0.99].

Step 2: The fitness value is evaluated based on (15). On this basis, the minimum results and the related values of α and β can be obtained.

Step 3: If the fitness value is better than $pbest_{ij}^k$ in the history, the current value is defined as a new $pbest_{ij}^k$. Meanwhile, $gbest_{ij}^k$ is replaced by the new particle with the best fitness value of all the particles.

Step 4: The velocity of different particles should be recalculated by (16). All of the particles should be removed to their new positions based on (17).

Step 5: If the maximum iterations or global optimization goal is satisfied, the PSO program should be terminated. Otherwise, it should repeat the procedures from Step 2 to Step 5.

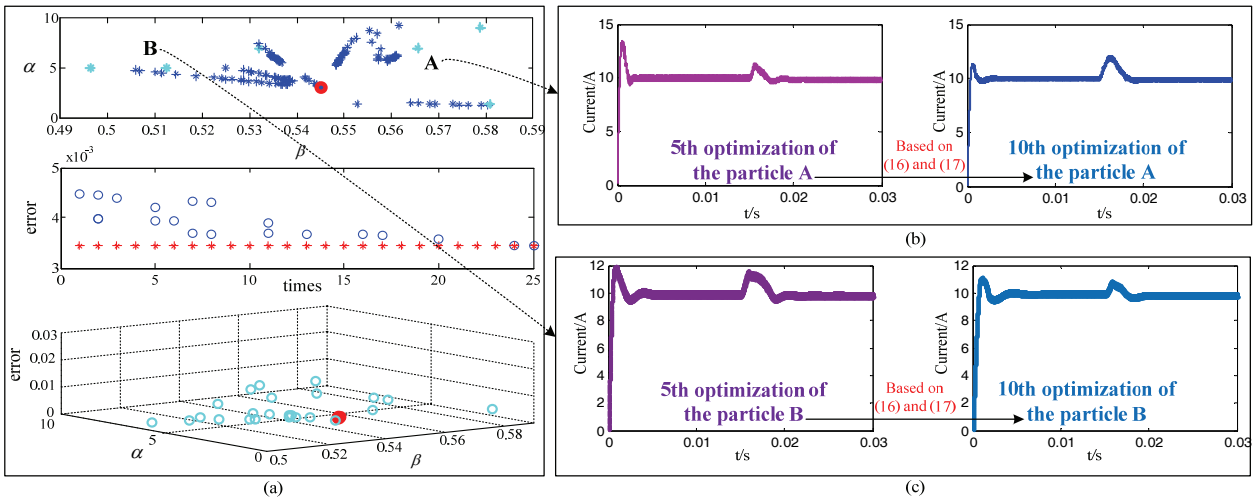

Fig. 6. Results of the PSO algorithm and the corresponding control effects. (a) Results of the PSO algorithm. (b) Control effects in accordance with the 5th/10th optimization of A. (c) Control effects in accordance with the 5th/10th optimization of B.

V. Results and Analysis

A. Simulation Results and Discussion

The parameters of the boost converter based HPS are $L=850$ uH, $C=60$ uF and $V_{bat}=25$ V. The rated voltage and capacitance parameters of the SC are 60 V and 15.6 Farads, respectively. The parameters of the ASMC controller are designed as $\beta_1=0.15$, $\beta_2=200$, $\lambda=10$, $k_1=30$ and $k_2=200$. For the PSO algorithm, the maximum number of iterations is equal to 25, $c_1=0.352$, $c_2=0.132$ and ω=0.579. The simulation results of the PSO algorithm are shown in Fig. 6(a). Based on the simulation results, the two optimal exponential gains should be designed as $\alpha=3$ and $\beta=0.545$.

To show the optimization process of the PSO for the ASMC system, the current control effects in accordance with the 5th and 10th optimization of particles A and B are illustrated in Fig. 6(b) and 6(c). It can be seen that the sub-optimization results of A and B are updated continuously by the PSO. The sub-optimization results of A and B are in accordance with the parameters α and β so that the corresponding duty ratio in (14) can be continuously optimized. In the simulation and experiment, a constant-frequency PWM signal with the duty ratio in (14) is used to control the MOSFET of the boost converter. On this basis, the control effects of the ASMC controller based on the optimization results of A and B can be obtained.

The control effect in accordance with the 10th optimization of particle A is better than that of the 5th optimization under the start-up condition. However, the control effect is degraded under the load variation condition. Actually, the value of the global optimization goal function in (15) is reduced. Therefore, the comprehensive control effect is improved for particle A. As a comparison, for particle B, it can be seen that the control effect in accordance with the 10th optimization can be effectively improved under start-up and load variation conditions when compared with the 5th optimization. These simulation results also demonstrate that the control effect cannot be regularly improved by simply increasing or decreasing the two exponential gains.

In order to verify the effectiveness of the proposed ASMC strategy with the EORL for a boost converter based HPS, ASMC strategies with different reaching laws are simulated. The comparative simulation results are shown in Fig. 7. In the simulations, the reference current is 10 A. The initial load resistor is 10 Ω. When compared with the ASMC strategy with the conventional reaching law (CRL) $u_{SMC}=-ks(t)-\rho\,\mathrm{sgn}(s(t))$, the proposed ASMC strategy with the EORL has nearly a 32.5% settling-time improvement in terms of the start-up current adjustment. The corresponding current overshoot can be reduced by up to 23%.

If the reaching law is $\dot{s}_2=-k_2|s|^{\beta}\,\mathrm{sgn}(s)-\varepsilon\,\mathrm{sgn}(s)$, i.e., the ASMC strategy is designed with only the fractional reaching law (FRL), the control performance is degraded when compared with the proposed ASMC strategy with the EORL for start-up current adjustment. According to the authors of [20], the start-up current adjustment becomes faster with an increased value of β. Therefore, the item $-k_1s^{\alpha}$ can be considered as an increased value of β in the reaching law ($u_{SMC}=-k_1s^{\alpha}-k_2|s|^{\beta}\,\mathrm{sgn}(s)-\varepsilon\,\mathrm{sgn}(s)$) of the proposed ASMC strategy. Simulation results show that the proposed ASMC strategy with the EORL can effectively improve the start-up current adjustment performance.

Fig. 7 also shows the robustness of the ASMC strategy with different reaching laws to deal with load variations. The load variation is changed from 10 Ω to 5 Ω. Since the SC voltage is

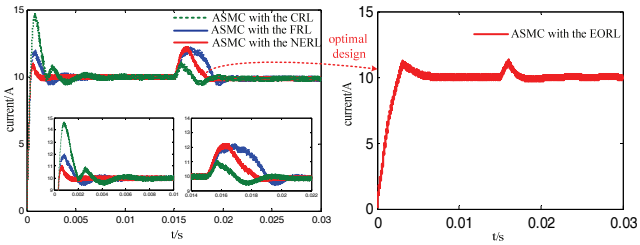

Fig. 7. Simulation of the ASMC with different reaching laws.

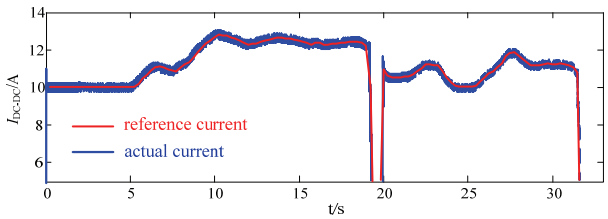

Fig. 8. Simulated global current tracking control effect of the ASMC strategy with the EORL.

50 V, the output power of the boost converter based HPS is changed from 250 W to 500 W. It can be seen that the current adjustment effect cannot be improved if the ASMC strategy is implemented with a non-optimal exponential reaching law (NERL). In fact, the current control effect is even worse than that of the ASMC strategy with the CRL. However, if the ASMC strategy with the EORL is implemented, it has up to 25% and 40% settling-time improvements of the current adjustment during a load change when compared to the ASMC strategy with the CRL and the ASMC strategy with the FRL, respectively. In addition, the current overshoot can be effectively suppressed.

To demonstrate that the proposed ASMC strategy with the EORL can achieve robust current tracking control for the boost converter based HPSs in EV applications, a global current tracking control effect of the proposed ASMC strategy with the EORL is also simulated, as shown in Fig. 8.

The reference current is given based on a small EV test in the laboratory. It can be seen that the actual current can satisfactorily track the reference current. Current overshoot only occurs when the boost converter operates under the start-up condition. The current shock can be regulated and suppressed to within 1 A. In addition, the output current of the boost converter is very smooth. In summary, the simulation results show that the proposed ASMC strategy with the EORL can improve the current adjustment performance to deal with load variations. In EV applications, the proposed ASMC strategy with the EORL has an excellent current tracking control effect for boost converter based HPSs.

B. Experimental Results and Discussion

An experimental platform is established for testing the control performance of the proposed ASMC strategy with the EORL, as shown in Fig. 9.

In the experiment, the ASMC strategy with the EORL is

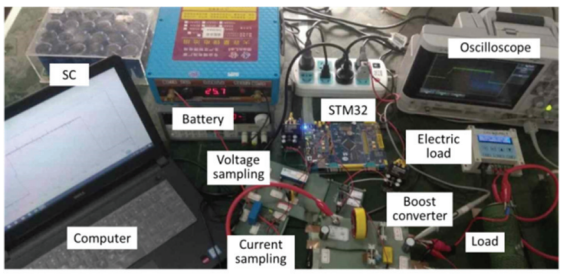

Fig. 9. Experimental platform.

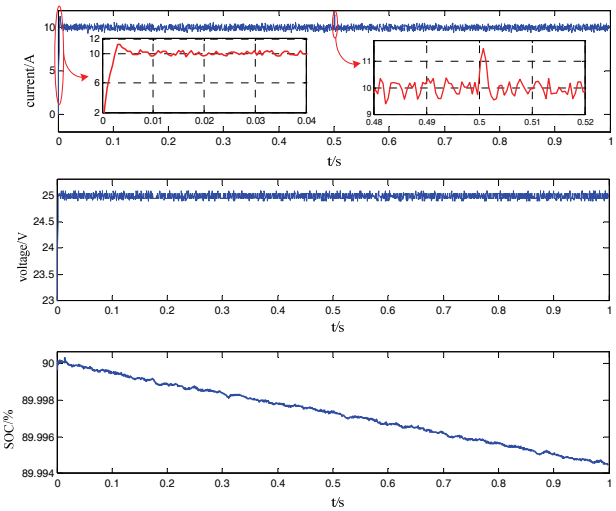

Fig. 10. Experimental results of a battery in the HPS.

implemented via a STM32 controller. The initial voltages of the SC and the battery are 45 V and 25.5 V, respectively. The reference current is 10 A. To ensure the system safety of the boost converter based HPS, only the final optimal results are used to control the boost converter based HPS in the experiment.

Fig. 10 shows experimental results of the battery under start-up and load variation conditions. The load change is from 10 Ω to 5 Ω, i.e., the output power of the boost converter based HPS is changed from 202.5 W to 405 W. When the boost converter based HPS is controlled by the ASMC strategy with the EORL, a fast dynamic current response can be achieved for the boost converter under start-up and load variation conditions. The results in Fig. 10 are obtained by a STM32 controller which is connected to a current sensor and a voltage sampling circuit. The battery SOC is calculated based on the battery voltage.

The duty ratio can be adaptively reduced when a large resistor is loaded, as shown in Fig. 11. By combining this with the experimental results in Fig. 10, it can be seen that the convergence time is less than 10 ms. That is to say, the finite time convergence of the proposed ASMC strategy with the EORL can be assured. In summary, the proposed ASMC strategy with the EORL can achieve robust current tracking control for boost converter based HPSs.

In Fig. 12, it is shown that the SC can provide peak power

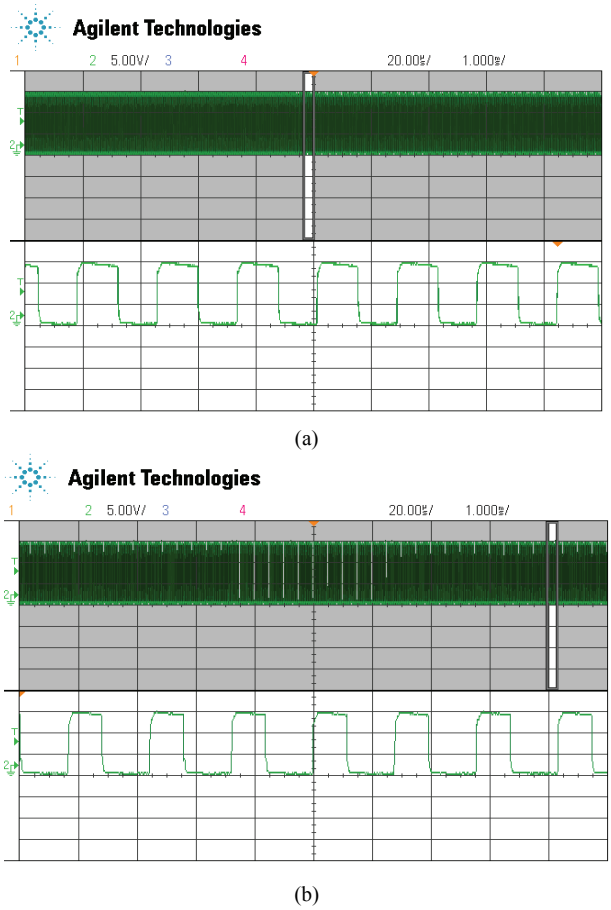

(a)

(b)

Fig. 11. Adaptive adjustment of the duty ratio. (a) Duty ratio before a load change. (b) Duty ratio after a load change.

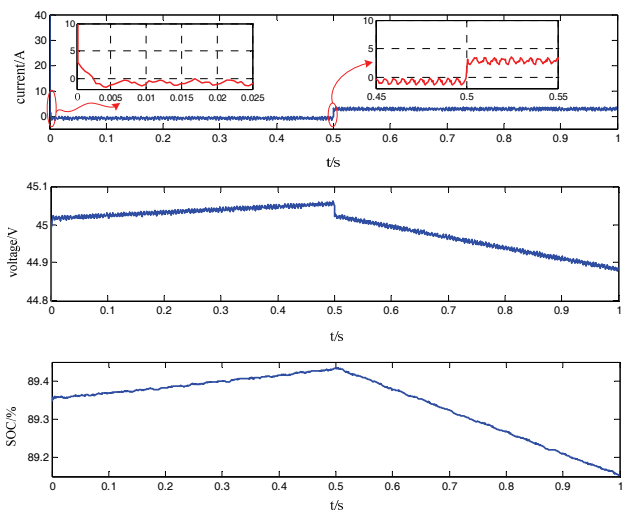

Fig. 12. Experimental results of the SC in the HPS.

under the start-up condition. If the load resistance is small, the SC is charged so that its voltage continues to rise. However, the SC is discharged if a large resistance is loaded. As a result, the SC voltage drops consistently. According to the sampling data of the STM32 controller, the SC SOC can be calculated based on the SC voltage. Based on the ASMC strategy with the

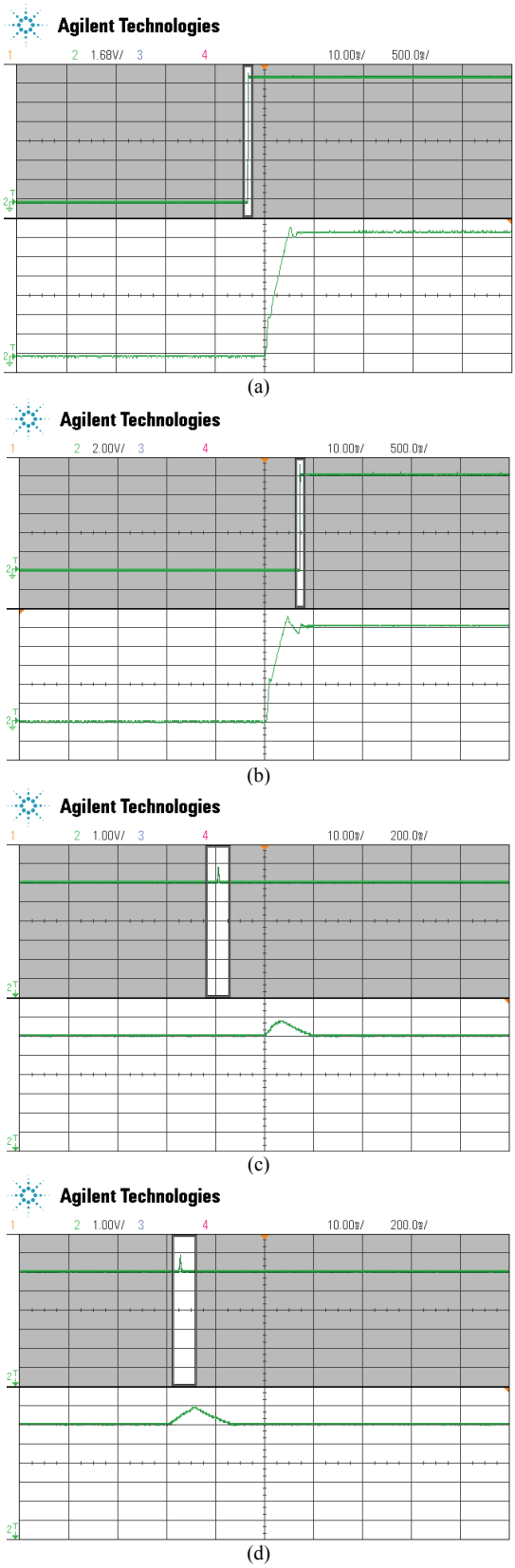

(a)

(b)

(c)

(d)

Fig. 13. Comparative results of two ASMC strategies. (a) Start-up response of the ASMC strategy with the EORL. (b) Start-up response of the conventional ASMC strategy. (c) Load change-response of the ASMC strategy with the EORL. (d) Load change-response of the conventional ASMC strategy.

TABLE I
COMPARATIVE ANALYSIS OF TWO ASMC STRATEGIES

ASMC strategy with the EORL		Conventional ASMC strategy	
Start-up	Load variation	Start-up	Load variation
7.16 ms	9.32 ms	8.91 ms	13.58 ms

EORL, the SC can provide peak power to the load and absorb extra output power from the battery. According to experimental results, the battery can operate with a constant power/current so that the system stability and the battery safety can be guaranteed. Therefore, the proposed ASMC with the EORL is very valuable for the operation stability and security of boost converter based HPSs.

To have a quantitative evaluation of the ASMC strategy with the EORL, the conventional ASMC strategy is also implemented in the experimental platform. The load is changed from 5 Ω to 2.5 Ω. The output power of the boost converter based HPS increases from 405 W to 810 W. Fig. 13 and Table I show comparative results of the two ASMC strategies. When compared with the conventional ASMC strategy, the convergence time of the proposed ASMC strategy with the EORL can be improved by up to 19.6% and 31.3% under start-up and load variation conditions, respectively. In addition, the current amplitude of the boost converter in the HPS can be effectively improved under the start-up condition. The experimental results shown in Fig. 13 are in accordance with the simulation results of the ASMC with the EORL in Fig. 7.

To make the proposed ASMC strategy with the EORL for the boost converter based HPSs in EVs become more persuasive, a comprehensive experiment in a small EV is implemented. In this experiment, the energy management of a boost converter based HPS in a small EV is designed according to [3]. Experimental results are shown in Fig. 14.

Current shock only occurs when the boost converter operates under the start-up condition. When the ASMC strategy with the EORL is used to control the boost converter based HPS in the small EV, the current shock can be effectively suppressed. In addition, it is evident that the SC can provide peak power to the motor inverter when the boost converter operates under the start-up condition. Moreover, the SC can effectively respond to the power demand. In addition, it can provide peak power to or absorb extra power from the motor inverter. On this basis, the battery only needs to provide constant or compensation power to the motor inverter.

The obtained experimental results are basically in accordance with the simulation results, i.e., the operating current can track the reference current in both the simulation and the experiment. Current shock can be effectively suppressed within 1 A. The experimental results are slightly different than the simulation results since some insignificant parameters of the boost converter were ignored in the simulation model. These ignored parameters have little impact on the global current tracking control effect of the boost converter based HPS. Therefore, the active and stable

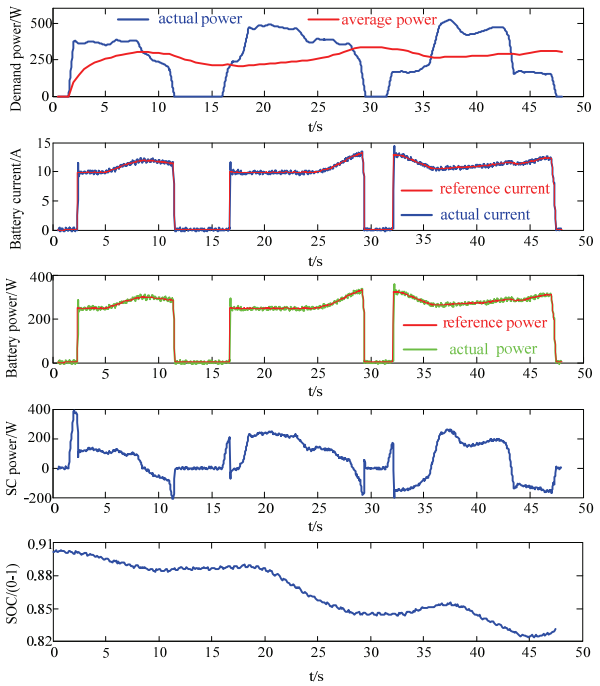

Fig. 14. Comprehensive results of the boost converter based HPS controlled by the ASMC strategy with the EORL.

power distribution of the boost converter based HPS can be effectively guaranteed in EV applications.

VI. CONCLUSIONS

This paper designed an ASMC strategy with an EORL for the robust current tracking control of boost converter based HPSs in EVs. By using the EORL, the proposed ASMC strategy can improve convergence time and current amplitude of the boost converter based HPS when compared with conventional ASMC strategies. The conventional ASMC strategy was designed based on state observers and the HC method. On this basis, a novel enhanced exponential reaching law was proposed for improving the ASMC strategy. Furthermore, a PSO algorithm was introduced to optimize the enhanced exponential reaching law. The final adaptive control factor was redesigned based on the EORL.

A simulation model of the boost converter based HPS controlled by the proposed ASMC strategy with the EORL was established. The obtained simulation results showed that the proposed ASMC strategy with the EORL had an excellent current tracking control effect for the boost converter based HPS. Moreover, an experimental platform was constructed to verify the effectiveness of the ASMC strategy with the EORL. When compared with the conventional ASMC strategy, the proposed ASMC strategy with the EORL improved the convergence time of current adjustment by up to 19.6% and 31.3% for the boost converter based HPS under start-up and load variation conditions, respectively. In addition, experimental results showed that the current overshoot of the boost

converter based HPS can be effectively suppressed to a reasonable range. In summary, the proposed ASMC strategy with the EORL can achieve robust current tracking control for the boost converter based HPSs in EV applications. It can guarantee the active and stable power distribution of boost converter based HPSs.

ACKNOWLEDGMENT

This work was supported by the Postdoctoral Science Foundation of China (Grant No. 2018M631143), the National Natural Science Foundation of China (Grant No. 21808179) and the Nature Science Basic Research Plan in Shaanxi Province of China (Grant No. 2018JQ5126).

REFERENCES

[1] B. Hredzak, V. G. Agelidis, and G. Demetriades, "Application of explicit model predictive control to a hybrid battery-ultracapacitor power source," *J. Power Sources*, Vol. 277, pp. 84-94, Mar. 2015.

[2] Z. Song, J. Li, J. Hou, H. Hofmann, M. Ouyang, and J. Du, "The battery-supercapacitor hybrid energy storage system in electric vehicle applications: A case study," *Energy*, Vol. 154, pp. 433-441, Jul. 2018.

[3] B. Wang, J. Xu, D. Xu, and Z. Yan, "Implementation of an estimator-based adaptive sliding mode control strategy for a boost converter based battery/supercapacitor hybrid energy storage system in electric vehicles," *Energy Conversion and Management*, Vol. 151, pp. 562-572, Nov. 2017.

[4] B. Wang, J. Xu, R. J. Wai, and B. Cao, "Adaptive sliding-mode with hysteresis control strategy for simple multi-mode hybrid energy storage system in electric vehicles," *IEEE Trans. Ind. Electron*., Vol. 64, No. 2, pp. 1404-1414, Feb. 2017.

[5] Z. Song, H. Hofmann, J. Li, X. Han, and M. Ouyang, "Optimization for a hybrid energy storage system in electric vehicles using dynamic programing approach," *Applied Energy*, Vol. 139, pp. 151-162, Feb. 2015.

[6] T. K. Santhosh，K. Natarajan, and C. Govindaraju, "Synthesis and implementation of a multi-port DC/DC converter for hybrid electric vehicles," *J. Power Electron*., Vol. 15, No. 5, pp. 1178-1189, Sep. 2015.

[7] B. Wang, J. Xu, B. Cao, and X. Zhou, "A novel multimode hybrid energy storage system and its energy management strategy for electric vehicles," *J. Power Sources*, Vol. 281, pp. 432-443, May 2015.

[8] G. Ren, G. Ma, and N. Cong, "Review of electrical energy storage system for vehicular applications," *Renew. Sustain. Energy Rev.*, Vol. 41, pp. 225-236, Jan. 2015.

[9] Z. Song, J. Hou, H. Hofmann, J. Li, and M. Ouyang, "Sliding-mode and Lyapunov function-based control for battery/supercapacitor hybrid energy storage system used in electric vehicles," *Energy*, Vol. 122, pp. 601-612, Mar. 2017.

[10] B. Wang, J. Xu, B. Cao, and B. Ning, "Adaptive mode switch strategy based on simulated annealing optimization of a multi-mode hybrid energy storage system for electric vehicles," *Applied Energy*, Vol. 194, pp. 596-608, May 2017.

[11] M. C. Mira, Z. Zhang, A. Knott, and M. A. E. Andersen, "Analysis, design, modeling, and control of an interleaved-boost full-bridge three-port converter for hybrid renewable energy systems," *IEEE Trans. Power Electron*., Vol. 32, No. 2, pp. 1138-1155, Feb. 2017.

[12] D. B. W. Abeywardana, B. Hredzak, and V. G. Agelidis, "A fixed-frequency sliding mode controller for a boost-inverter-based battery-supercapacitor hybrid energy storage system," IEEE Trans. Power Electron., Vol. 32, No. 1, pp. 668-680, Jan. 2017.

[13] T. A. F. Theunisse, J. Chai, R. G. Sanfelice, and W. P. M. H. Heemels, "Robust global stabilization of the DC-DC boost converter via hybrid control," *IEEE Trans. Circuits Syst. I, Reg. Papers*, Vol. 62, No. 4, pp. 1052-1061, Apr. 2015.

[14] C. Yfoulis, D. Giaouris, F. Stergiopoulos, C. Ziogou, S. Voutetakis, and S. Papadopoulou, "Robust constrained stabilization of boost DC–DC converters through bifurcation analysis," *Contr. Eng. Practice*, Vol. 35, pp. 67-82, Feb. 2015.

[15] N. Mukherjee and D. Strickland, "Control of cascaded DC-DC converter-based hybrid battery energy storage systems - Part II: Lyapunov approach," *IEEE Trans. Ind. Electron.*, Vol. 63, No. 5, pp. 3050-3059, May 2016.

[16] A. Beddar, H. Bouzekri, B. Babes, and H. Afghoul, "Experimental enhancement of fuzzy fractional order PI+I controller of grid connected variable speed wind energy conversion system," *Energy Convers. Manag.*, Vol. 123, pp. 569-580, Sep. 2016.

[17] R. J. Wai and L. C. Shih, "Adaptive fuzzy-neural-network design for voltage tracking control of a DC–DC boost converter," *IEEE Trans. Power Electron*., Vol. 27, No. 4, pp. 2104-2115, Apr. 2012.

[18] E. Nechadi, M. N. Harmas, A. Hamzaoui, and N. Essounbouli, "A new robust adaptive fuzzy sliding mode power system stabilizer*," Int. J. Electr. Power Energy Syst*., Vol. 42, pp. 1-7, Nov. 2012.

[19] M. Li, H. Xu, W. Li, Y. Liu, F. Li, Y. Hu, and L. Liu, "The structure and control method of hybrid power source for electric vehicle," *Energy*, Vol. 112, pp. 1273-1285, Oct. 2016.

[20] H. Komurcugil, "Non-singular terminal sliding-mode control of DC–DC buck converters," *Contr. Eng. Practice*, Vol. 21, No. 3, pp. 321-332, Mar. 2013.

[21] Z. Wang, Y. Mao, Z. Hu, and Y. Xie, "A sliding mode control design based on the reaching law for matrix rectifiers," *J. Power Electron*., Vol. 16, No. 3, pp. 1122-1130, May 2016.

[22] X. Hao, X. Yang, T. Liu, L. Huang, and W. Chen, "A sliding-mode controller with multiresonant sliding surface for single-phase grid-connected VSI with an LCL filter," *IEEE Trans. Power Electron*., Vol. 28, No. 5, pp. 2259-2268, May 2013.

[23] S. Oucheriah and L. Guo, "PWM-based adaptive sliding-mode control for boost DC–DC converters," *IEEE Trans. Ind. Electron*., Vol. 60, No. 8, pp. 3291-3294, Aug. 2013.

[24] H. Afghoul, F. Krim, B. Babes, A. Beddar, and A. Kihel, "Design and real time implementation of sliding mode supervised fractional controller for wind energy conversion system under sever working conditions," *Energy Convers. Manag*., Vol. 167, pp. 91-101, Jul. 2018.

[25] L. Xu, J. Hu, S. Cheng, C. Fang, J. Li, M. Ouyang, and W. Lehnert, "Nonlinear observation of internal states of fuel cell cathode utilizing a high-order sliding-mode algorithm," *J. Power Sources*, Vol. 356, pp. 56-71, Jul. 2017.

[26] K. Zheng, G. Zhang, D. Zhou, J. Li, and S. Yin, "Modeling, dynamic analysis and control design of full-bridge LLC resonant converters with sliding-mode and PI control scheme," *J. Power Electron*., Vol. 18, No. 3, pp. 766-777, May 2018.
[27] H. Yu, D. Tarsitano, X. Hu, and F. Cheli, "Real time energy management strategy for a fast charging electric urban bus powered by hybrid energy storage system," *Energy*, Vol. 112, pp. 322-331, Oct. 2016.
[28] Z. Li, C. Zang, P. Zeng, H. Yu, S. Li, and J. Bian, "Control of a grid-forming inverter based on sliding mode and mixed H2/H∞ control," *IEEE Trans. Ind. Electron*., Vol. 64, No. 5, pp. 3862-3872, May 2017.
[29] V. Repecho, D. Biel, J. M. Olm, and E. Fossas, "Switching frequency regulation in sliding mode control by a hysteresis band controller," *IEEE Trans. Power Electron*., Vol. 32, No. 2, pp. 1557-1569, Feb. 2017.
[30] R. J. Wai and L. C. Shih, "Design of voltage tracking control for DC-DC boost converter via total sliding-mode technique," *IEEE Trans. Ind. Electron*., Vol. 58, No. 6, PP.2502-2511, Jun. 2011.
[31] C. Mu and H. He, "Dynamic behavior of terminal sliding mode control," *IEEE Trans. Ind. Electron*., Vol. 65, No. 4, pp. 3480-3490, Apr. 2018.
[32] T. Mesbahi, F. Khenfri, N. Rizoug, P. Bartholomeüs, and P. L. Moigne, "Combined optimal sizing and control of Li-Ion battery/supercapacitor embedded power supply using hybrid particle swarm–nelder–mead algorithm," *IEEE Trans. Sustain. Energy*, Vol. 8, No. 1, pp. 59-73, Jan. 2017.
[33] Z. Chen, R. Xiong, and J. Cao, "Particle swarm optimization-based optimal power management of plug-in hybrid electric vehicles considering uncertain driving conditions," *Energy*, Vol. 96, pp. 197-208, Feb. 2016.
[34] X, Guo, H. Ren, and D. Liu, "An optimized PI controller design for three phase PFC converters based on multi-objective chaotic particle swarm optimization," *J. Power Electron*., Vol. 16, No. 2, pp. 610-620, Mar. 2016.
[35] S. W. Fei, M. J. Wang, Y. B. Miao, J. Tu, and C. L. Liu, "Particle swarm optimization-based support vector machine for forecasting dissolved gases content in power transformer oil," *Energy Convers. Manag*., Vol. 50, pp. 1604-1609, Jun. 2009.
[36] T. T. Song and S. H. Chung, "Boundary control of boost converters using state-energy plane," *IEEE Trans. Power Electron*., Vol. 23, No. 2, pp. 551-563, Mar. 2008.

Bin Wang was born in Guangxi, China, in 1987. He received his B.S. degree in Automation Engineering and his M.S. degree in Control Science and Engineering from the Henan University of Science and Technology, Luoyang, China, in 2010 and 2013, respectively. He received his Ph.D. degree in Mechanical Engineering from Xi'an Jiaotong University, Xi'an, China, in 2017. He is presently a Research Associate in School of Mechanical Engineering, Xi'an Jiaotong University. His current research interests include energy storage systems, electric vehicles, and dc-dc converter control.

Chaohui Wang received his M.S. and Ph.D. degrees from Xi'an Jiaotong University, Xi'an, China, in 1998 and 2003, respectively. He is presently working as a Professor in School of Mechanical Engineering, Xi'an Jiaotong University. His current research interests include mechatronic systems, MEMS, microfluidics, and surface acoustic waves.

Qiao Hu received his M.S. and Ph.D. degrees from Xi'an Jiaotong University, Xi'an, China, in 2003 and 2006, respectively. He is presently a Research Fellow in the School of Mechanical Engineering, Xi'an Jiaotong University. His current research interests include the coordination control of underwater electric vehicles, automatic control, and fault diagnosis of mechatronic systems.

Guangliang Ma was born in Henan, China, in 1994. He received his B.S. degree in Information Engineering from Xi'an Jiaotong University, Xi'an, China, in 2016, where he is presently working towards his M.S. degree in the School of Mechanical Engineering. His current research interests include the energy management of electric vehicles and dc-dc converter control.

Jiahui Zhou was born in Zhejiang, China, in 1994. He received his B.S. degree in Vehicle Engineering from Southwest Jiaotong University, Sichuan, China, in 2017. He is presently working towards his M.S. degree in the School of Mechanical Engineering, Xi'an Jiaotong University, Xi'an, China. His current research interests include the control and energy management of hybrid energy storage systems in electric vehicles.